

Chapter 6: Cellular Processing of Rhodium Metalloinsertors: Investigations into the Underlying Biological Mechanisms Involved in Response to Mismatch Recognition*

6.1 Introduction

DNA replication is essential for cell growth and reproduction, and ensuring the fidelity of the genome is vital for the survival of all organisms. DNA defects occur naturally during replication and as a result of chemical damage. Unchecked DNA damage can cause further mutations that lead to cellular dysfunction and disease. Specifically, single-strand defects such as mismatches, abasic sites, and oxidized bases are associated with elevated mutation rates and carcinogenesis.¹ To correct these errors and increase the fidelity of replication, cells have evolved a complex repair pathway involving nucleotide excision repair (NER), base excision repair (BER), and mismatch repair (MMR).²

The MMR machinery recognizes and repairs single base lesions that arise from errors in DNA replication.^{3,4} Deficiencies in the MMR machinery increase the rates of mutagenesis 50-1000 fold,^{5,6} a hallmark of MMR-deficiency is microsatellite instability, which refers to the gain or loss of mono-, di-, or tri-nucleotide repeat sequences within the genome.⁷ Microsatellite instability arises from uncorrected frame-shift mutations that occur during replication and is associated with human diseases such as xeroderma pigmentosum and colorectal cancer.^{8,9} In fact, mismatch repair deficiencies have been

**Acknowledgments:* Julie Bailis (Amgen) prepared the tumor samples from the *in vivo* mouse studies. Professor Jeremy Stark, Diana Yanez (City of Hope), and Kelsey Boyle (Caltech) assisted with the immunofluorescence assay and collected images by fluorescence microscopy. Kelsey Boyle also assisted with quantitative analysis of the fluorescence data. I synthesized the metalloinsertors, performed lysis and analysis of tumor samples for rhodium content by ICP-MS, carried out all HCT116 cell culture and fixation, and performed the transcription assay in the HCT116N and HCT116O cell lines.

found in approximately 80% of hereditary nonpolyposis colon cancer cases and in 16% of all solid tumors.^{9,10} Additionally, MMR-deficient cancers exhibit resistance to common chemotherapeutics such as DNA alkylators and platinating agents, as MMR proteins are responsible for recognizing the DNA adducts formed by these agents.^{11,12} The deleterious effects of MMR deficiency have demonstrated a need to develop therapeutic agents that target MMR-deficient cancers.

The development of transition metal-based chemotherapeutic agents burgeoned with the discovery of the anti-cancer properties of *cis*-dichlorodiammineplatinum (II) (cisplatin). While later generations of inorganic therapeutics have been developed with enhanced potency, the field has increasingly turned towards the development of more targeted therapies. The design of compounds that can selectively target biomarkers of cancer aims to achieve potency specifically in malignant cells over healthy cells, thus mitigating side effects arising from off-target toxicity. In recent years, inorganic compounds have been exploited for their complex geometries, stereoselectivity, and rich photochemistry in the selective targeting of DNA, proteins, and organelles that have been implicated in carcinogenesis.¹³

Our laboratory has focused on the design of octahedral rhodium (III) complexes bearing sterically expansive ligands for the selective targeting of DNA mismatches. Benzo-fused expansion of traditional intercalating ligands precludes the intercalative binding mode, resulting in exclusive targeting of thermodynamically destabilized sites.¹⁴ These complexes – dubbed “metalloinsertors” due to the complete extrusion of the mismatched base pairs from the helix and consequent insertion of the planar ligand in the

intervening space – target destabilized sites in DNA with over 1000-fold precision *in vitro*.¹⁵⁻¹⁸

The potential of rhodium metalloinsertors to recognize mismatches *in vivo* has been extensively explored. The nature of the metalloinsertion binding mode, wherein the metal complex approaches from the minor groove and ejects the mismatched bases out into the major groove, is hypothesized to create a large lesion that could be recognized by proteins in the cell.^{15,16,19} The biological activity of metalloinsertors has been characterized primarily in two isogenic cell lines derived from the HCT116 human colorectal carcinoma line. Wild-type HCT116 cells are deficient in the MLH1 protein, an essential component of the MMR protein complex. The HCT116N daughter cell line is transfected with a copy of human chromosome 3 (ch3), which encodes the *hMLH1* gene; these cells express MLH1 and restore functional mismatch repair. The HCT116O line is transfected with a copy of chromosome 2 (ch2), resulting in an isogenically matched daughter line that remains MMR-deficient.²⁰ Metalloinsertors have been shown to inhibit cell proliferation^{21,22} and induce cytotoxicity selectively in the MMR-deficient HCT116O cell line, and these cytotoxic effects proceed via a necrotic pathway.²³ Moreover, it has been shown that this cell-selectivity arises from localization of complexes to the nucleus, whereas cell death occurs indiscriminately in both cell lines upon localization to the mitochondria.^{24,25} These results support the notion that nuclear DNA is the preferred biological target of our rhodium complexes, rather than the mitochondrial genome.

The isogenically matched HCT116N and HCT116O cell lines have proven extremely useful in elucidating the mismatch sensitivity of metalloinsertors in cells. Given the dependence of cell-selective toxicity on nuclear targeting in addition to the

absence of the critical MMR protein MLH1, which repairs genomic but not mitochondrial DNA, it is feasible to conclude that the biological activity of metalloinsertors is the result of mismatch recognition within the genome. This was further validated in a recent study involving NCI-H23 lung adenocarcinoma cells that contain a doxycycline-inducible short hairpin RNA (shRNA) that suppresses expression of the MLH1 gene. This not only enabled mismatch repair to be turned on and off within the same cell line, but also removed the potential for interference arising from chromosomal instability, which can occur in the HCT116 daughter lines that have been transfected with an entire additional chromosome. The selectivity of metalloinsertors for MMR-deficiency in the inducible cell line refutes the notion that the biological activity of metalloinsertors is the result of off-target effects within the cell.²⁶

As new generations of metalloinsertors are developed with increasing potency and selectivity, we consider their potential as clinically viable alternatives to the current repertoire of treatments of MMR-related cancers. However, we still understand relatively little about the underlying mechanisms surrounding rhodium mismatch recognition in the genome. The cellular processing and downstream effects that occur in the period between the initial DNA binding event and the first stages of necrosis remain largely unclear. We have employed various fluorescence methods to probe the potential cellular pathways that may be activated in response to metalloinsertor treatment in the HCT116N and HCT116O cell lines. It has been discovered that metalloinsertors display evidence of inducing DNA strand breaks in the genome, eliciting the phosphorylation of histone H2AX (γ H2AX), which recruits DNA damage response and repair proteins.²⁷ Notably, we have observed cell-selective inhibition of transcription in MMR-deficient cells in

response to rhodium treatment, but not cisplatin. Finally, preliminary *in vivo* experiments in nude mice implanted with HCT116 tumor xenografts have revealed moderate toleration of rhodium as well as tumor uptake of metalloinsertors. Overall, it was determined that these complexes provoke a variety of rapid cellular responses at low doses and exhibit enormous potential for activity in complex biological systems.

6.2 Experimental Protocols

6.2.1 Materials

Cisplatin and all organic reagents were purchased from Sigma Aldrich unless otherwise noted. Commercially available chemicals were used as received without further purification. RhCl_3 starting material was purchased from Pressure Chemical Co (Pittsburgh, PA). Media and supplements were purchased from Invitrogen (Carlsbad, CA). Ethynyl uridine, Alexa Fluor 488®, copper sulfate, and associated buffers were purchased in kit form from Life Technologies (Carlsbad, CA). Vista Green DNA Dye, comet slides, and associated buffers and solutions were purchased in kit form from Cell Biolabs Inc. (San Diego, CA). An extraction kit for tumor cell lysis was purchased from Thermo Fisher Scientific (Waltham, MA). Antibodies for immunofluorescence assays were purchased from Abcam (Cambridge, UK).

The synthesis of 5,6-chryseno quinone (chrysi), 1-methyl-1-(pyridin-2-yl) ethanol (PPO), $[\text{Rh}(\text{HDPA})_2\text{chrysi}]\text{Cl}_3$, and $[\text{Rh}(\text{chrysi})(\text{phen})(\text{PPO})]\text{Cl}_2$ were carried out according to published protocols.^{22,28,29}

6.2.2 Cell Culture

HCT116N and HCT116O cells were grown in RPMI 1640 medium containing 10% FBS, 2 mM L- glutamine, 0.1 mM nonessential amino acids, 1 mM sodium

pyruvate, 100 units/mL penicillin, 100 µg/mL streptomycin, and 400 µg/mL Geneticin (G418). Cells were grown in tissue culture flasks (Corning Costar, Acton, MA) at 37 °C and 5% CO₂ humidified atmosphere.

6.2.3 Immunofluorescence Staining of Fixed Cells

6.2.3.1 Cell Treatment and Fixation

Immunofluorescence studies were carried out in 4-well chamber slides with removable walls. Slides were coated with 0.3 ml poly-L-lysine (Sigma) per chamber and incubated at 37 °C, 5% CO₂ for 90 minutes. The coating was aspirated, and HCT116N and HCT116O cells were seeded at 4×10^4 cells (0.5 ml media) per chamber. The slides were incubated at 37 °C under humidified atmosphere and given 24 h to adhere. Slides were treated with varying concentrations of [Rh(chrysi)(phen)(PPO)]²⁺ (0.1, 0.3, or 1 µM) or camptothecin (1 µM) for 2h at 37 °C. For time course experiments, drug-containing medium was aspirated after 2h, replaced with fresh medium, and allowed to grow at 37 °C for the appropriate durations. After the incubation period, the media was aspirated and cells were washed 2x with phosphate buffered saline (PBS, pH 7.2, 0.5 ml/chamber). Cells were fixed with 4% (w/v) paraformaldehyde in PBS (0.5 ml/chamber) for 15 min at room temperature. The fixative was aspirated and cells were washed 2x with PBS (0.5 ml each). Paraformaldehyde was quenched with 0.1 M glycine (0.5 ml/chamber) in PBS for 5 min at room temperature. The solution was removed by aspiration, and cells were washed with PBS (2 x 0.5 ml). For storage, 0.5 ml PBS was added to each chamber, and slides were stored at 4 °C until staining.

6.2.3.2 Immunofluorescence Staining

Cells were permeabilized with 0.5% Triton X-100 in PBS for 15 min, followed by aspiration and washing with 2 x 0.5 ml PBS. Cells were then blocked with 3 M bovine serum albumin (BSA) in PBS for 30 min. Primary antibodies were added (0.07 ml/chamber) as indicated in **Table 6.1** and incubated at 37 °C under humidified atmosphere for 2 h. Antibody solutions were removed and cells were washed with 2 x 0.5 ml PBS. Secondary antibodies were added (0.07 ml/chamber) as indicated in **Table 6.1** and incubated at 37 °C under humidified atmosphere for 1 h. Antibody was removed and cells were washed with 3 x 0.1 ml PBS for 5 min each (on rocker). Slides were then mounted with VECTASHIELD (1 drop/chamber) with DAPI. Slides were then dried at 4 °C overnight and imaged using fluorescence microscopy. Fluorescent images were captured using a Princeton Instruments cooled CCD digital camera from a Zeiss upright LSM 510 2-Photon confocal microscope.

6.2.3.3 Quantification and Analysis of Fluorescence Images

Fluorescent images were obtained as gray-scale data and false colorized with the corresponding dye colors using Photoshop. Quantitative analysis of protein focal accumulation (“foci”) was carried out using gray-scale images in a randomized double-blind study. Only cells with nuclei that were contained entirely within the image were counted – nuclei that were cut off at the edges were excluded from all quantitation. The numbers of foci per cell were denoted as negative (zero foci), low-staining (1-5 foci/cell), moderate-staining (6-10 foci/cell), or high-staining (>10 foci/cell). Cells displaying each type of foci were calculated as a percentage of the total cells in the collection of images for each sample. Between 3-5 images were collected for each chamber, ranging from ~30-150 cells total.

Table 6.1 Antibodies for Immunofluorescence Staining

Primary Antibody	Dilution	Secondary Antibody^a	Dilution
Mouse γ H2AX	1:500	Goat anti-mouse IgG	1:250
Rabbit FANCD2	1:250	Goat anti-rabbit IgG	1:250
Rabbit 53BP1	1:500	Goat anti-rabbit IgG	1:250
Mouse RPA	1:100	Goat anti-mouse IgG	1:250

^a Goat anti-mouse IgG secondary antibody contains an Alexa Fluor® 488 label ($\lambda_{\text{ex}} = 488$ nm). Goat anti-rabbit IgG secondary antibody contains an Alexa Fluor® 647 label ($\lambda_{\text{ex}} = 647$ nm).

6.2.4 MTT Cytotoxicity Assay

MTT experiments were performed with HCT116N and HCT116O cells as described in the literature.³⁰ HCT116N and HCT116O cells were inoculated with rhodium or camptothecin at varying concentrations and plated in 96-well plates at 50,000 cells/well. Cells were incubated for 72h at 37 °C under humidified atmosphere. After the incubation period, MTT was added, and the cells were incubated for an additional 4 h. The resulting formazan crystals were solubilized over a period of 24 h at 37 °C, 5% CO₂. Formazan formation was quantified *via* electronic absorption at 550-600 nm with a reference wavelength of 690 nm. Cell viability is expressed as a function of formazan formation and normalized to that of untreated cells. Standard errors were calculated from five replicates.

6.2.5 Comet Assay for Damage of Cellular DNA

Determination of rhodium-induced damage of genomic DNA was performed using the OxiSelect Comet Assay Kit (CellBioLabs). HCT116N and HCT116O cells were harvested by trypsinization and seeded in 6-well plates at 200,000 cells/well in 3 ml media. Cells were allowed 24 h to adhere at 37 °C under humidified atmosphere, followed by treatment with 500 nM of either camptothecin or [Rh(chrysi)(phen)(PPO)]²⁺. Untreated HCT116N and O cells were included as a control. Cells were grown for an additional 24 h and harvested by trypsinization. Cell pellets were washed with 3 ml cold PBS (pH 7.2) and resuspended in a minimal volume of PBS (~200 µl, ~4 x 10⁵ cells/ml). Cell suspensions were then combined with liquefied OxiSelect Comet Agarose (heated to 90 °C for 20 min and maintained at 37 °C prior to the experiment) at a 1:10 ratio (v:v), triturated via pipetting, and maintained at 37 °C until ready for plating. Immediately upon

removal from the 37 °C bath, the cell-agarose mixtures were triturated again and each pipeted onto a 3-well Comet Slide (75 µl/well). Slides were incubated at 4 °C in the dark for 15 min. Slides were then transferred to a basin containing pre-chilled Lysis buffer (2.5 M NaCl, 10 mM EDTA, 10 ml 10x Lysis solution from kit, 10 ml DMSO, Milli Q H₂O to 100 ml, pH 10) (25 ml/slide), and immersed at 4 °C in the dark for 30-60 min. The Lysis buffer was aspirated and replaced with pre-chilled Alkaline solution (300 mM NaOH, 1 mM EDTA, pH >13) at ~25 ml/slide for 30 min at 4 °C in the dark. The slides were then transferred to a horizontal electrophoresis chamber filled with 1 L of pre-chilled Alkaline Electrophoresis Buffer (300 mM NaOH, 1 mM EDTA, pH >13) and electrophoresed at ~20 V (450 mA) for 35 min. After electrophoresis, slides were washed with pre-chilled MilliQ water (2 x 25 ml for 2 min) followed by 70% EtOH (1 x 25 ml for 5 min). Slides were stored to dry at 4 °C in the dark until completely dry (~24 h).

For staining, a 10,000x solution of VistaGreen DNA dye was diluted to 1x in TE Buffer (10 mM Tris, pH 7.5, 1 mM EDTA) and added to each well (0.1 ml/well). Cells were protected with a coverslip and allowed to incubate at ambient temperature overnight while protected from light. Images were acquired by epi-fluorescence microscopy (excitation at 488 nm) using an Olympus IX81 with a 100× sapo objective with laser illumination at 532 nm. Fluorescent images were obtained as gray-scale data and false colorized green using Photoshop.

6.2.6 Assay for *In Cellulo* RNA Synthesis in HCT116N and O Cells

HCT116N and O cells were seeded in 96-well plates at 4×10^3 cells/well and allowed 24 h to adhere. After 24 h, cells were treated with 10 µl of 10x stock solutions of [Rh(chrysi)(phen)(PPO)]Cl₂ (0 – 1 µM final concentration) or cisplatin (0 – 10 µM final

concentration) at 37 °C under humidified atmosphere for 24 h. After the incubation period, an equal volume (100 µl) of 2 mM ethynyl uridine (EU) in pre-warmed media was added to each well, to a final concentration of 1 mM EU per well. EU pulse labeling was carried out at 37 °C under humidified atmosphere for 1 h. After the labeling period, the media was removed, and cells were fixed with 3.7% formaldehyde in phosphate buffered saline (PBS, pH 7.2) at 50 µl/well for 30 min at room temperature. The fixative was removed, and wells were washed 1x with 200 µl PBS (pH 7.2). Cells were then permeabilized with 0.5% Triton X-100 in PBS (pH 7.2) (50 µl/well for 15 minutes) and washed with PBS. A working solution of the Click-iT reaction cocktail was prepared immediately before treatment while protected from light, according to the manufacturer's instructions. The click reaction was carried out at ambient temperature for 30 minutes in the absence of light. The wells were aspirated and washed with the rinse buffer (50 µl/well). The plates were protected from light, and fluorescence readout of the wells was carried out on a Flexstation 3 Multi-Mode microplate reader (495 nm excitation, 519 nm emission, 515 nm automatic cutoff; top-read).

6.2.7 Animals

All breeding, housing, and treatment of mice were carried out at Amgen, Inc (Thousand Oaks, CA) in strict accordance with the recommendations in the Guide for the Care and Use of Laboratory Animals of the National Institutes of Health. Nude mice were implanted subcutaneously with HCT116 tumor cells. Once the tumors had grown to 50-250 mm³, mice were injected either intravenously (IV) or intraperitoneally (IP) with a single dose of rhodium (10, 20, or 100 mg/kg). Mice were sacrificed after 24h and tumors were harvested for rhodium analysis by ICP-MS.

6.2.8 Analysis of Tumor Samples for Rhodium Content by ICP-MS

Tumor samples were obtained from nude mice implanted with human HCT116 xenografts and homogenized manually at 4 °C. A nuclear protein extraction kit (Pierce from Thermo Scientific) was used for cell lysis. Nuclear and cytosolic lysates were separated from the insoluble fraction according to the manufacturer's instructions. The soluble fractions were combined and sonicated on a Qsonica Ultrasonic processor for 20 s at 40% amplitude. A 750 µl aliquot was diluted with 750 µl of a 2% HNO₃ (v/v) solution and analyzed for rhodium content by inductively coupled plasma mass spectrometry (ICP-MS) on an Agilent 8800 QqQ unit. The remainder of the cell lysate was analyzed for protein content *via* a bicinchoninic assay (BCA).³¹ Rhodium counts were normalized to protein content to obtain ng [Rh]/mg [protein].

6.3 Results

6.3.1 Immunofluorescence Staining of HCT116 Cells

Previous studies have established nuclear DNA as the preferred target of rhodium metalloinsertors for selective toxicity in MMR-deficient cells, but little is known about how the DNA-bound metalloinsertor is recognized and processed in the cell. Immunofluorescence staining was carried out on MMR-proficient HCT116N cells and MMR-deficient HCT116O cells to screen for the accumulation of proteins that localize to sites of DNA damage. Cells were plated in 4-well chamber slides and treated with either [Rh(chrysi)(phen)(PPO)]²⁺ or camptothecin (**Figure 6.1**), which induces double strand breaks in DNA,³² for 2h and either fixed or replaced with fresh media and allowed to

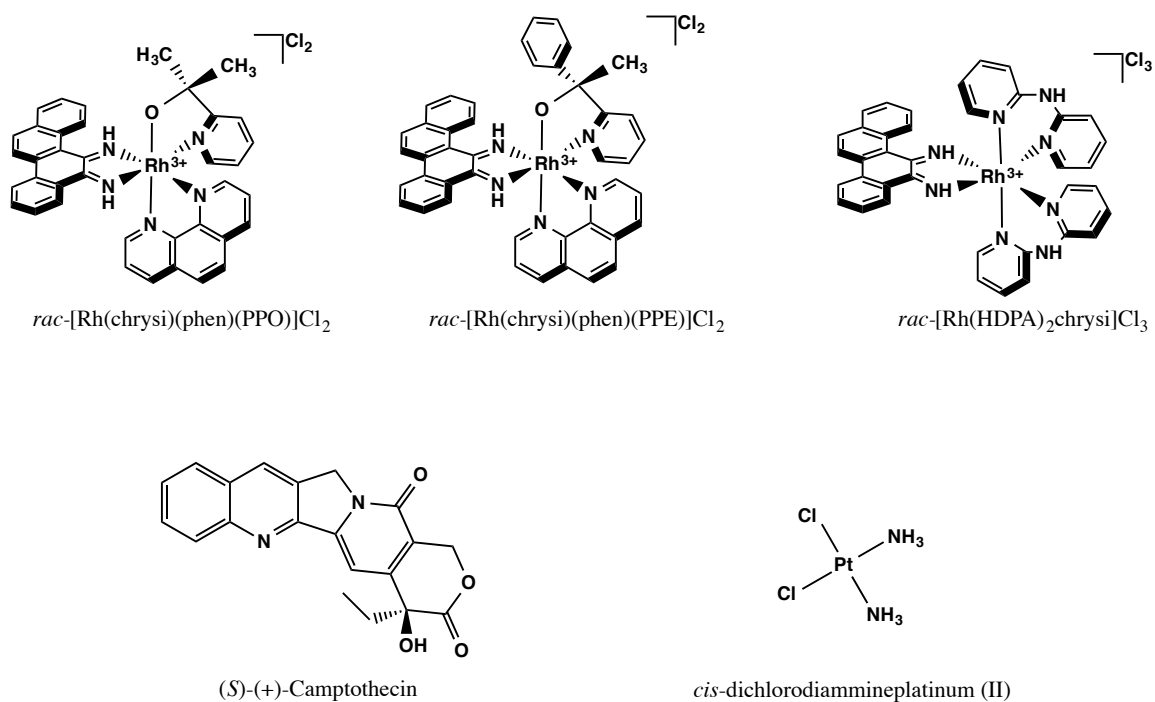


Figure 6.1 Chemical structures of complexes included in this study. Top (left to right): $[Rh(chrysi)(phen)(PPO)]^{2+}$, $[Rh(chrysi)(phen)(PPE)]^{2+}$ (included in *in vivo* studies), $[Rh(HDPA)_2chrysi]^{3+}$ (included in *in vivo* studies). Bottom (left to right): $(S)-(+)-Camptothecin$, which was employed as a control in immunofluorescence staining; cisplatin, which was used as a control in the transcription assay.

recover for periods of 6, 12, or 24h prior to fixation. Cells were then stained with antibodies for γ H2AX and p53-binding protein 1 (53BP1).

6.3.1.1 Induction of γ H2AX in HCT116 Cells

The focal accumulation of γ H2AX was examined in HCT116N and HCT116O cells in response to treatment with $[\text{Rh}(\text{chrysi})(\text{phen})(\text{PPO})]^{2+}$ for 2h followed by a cell fixation and immunofluorescence staining. Camptothecin-treated (1 μM) and untreated cells were included as controls. **Figure 6.2** shows the confocal immunofluorescence microscopy of HCT116O cells treated with rhodium (1 μM) and camptothecin and stained for γ H2AX. The focal accumulation of γ H2AX – known as “foci” – signifies the presence of double strand breaks (DSBs) in DNA.²⁷ These foci appear as punctate stains within the nucleus, indicating points of DNA damage. Nuclear co-staining with DAPI is shown in blue.

As can be seen in **Figure 6.2**, camptothecin displays characteristically high punctate staining of γ H2AX. $[\text{Rh}(\text{chrysi})(\text{phen})(\text{PPO})]^{2+}$ also induces γ H2AX foci comparable to that of camptothecin at the same concentration, and above the background fluorescence of untreated cells. The incidence of γ H2AX foci in rhodium-treated cells suggests that metalloinsertors may induce DSBs in the genome.

Immunofluorescence staining for γ H2AX was also carried out for HCT116N cells. At 1 μM rhodium, foci were detected in both cell lines. We postulated that differential fluorescence staining may be observed with lower concentrations of rhodium. Staining was carried out on HCT116N and HCT116O cells treated with 100 and 300 nM $[\text{Rh}(\text{chrysi})(\text{phen})(\text{PPO})]^{2+}$ for 2h. As can be seen in **Figure 6.3**, little difference could be observed between the two cell lines. Additionally, untreated cells display unusually high

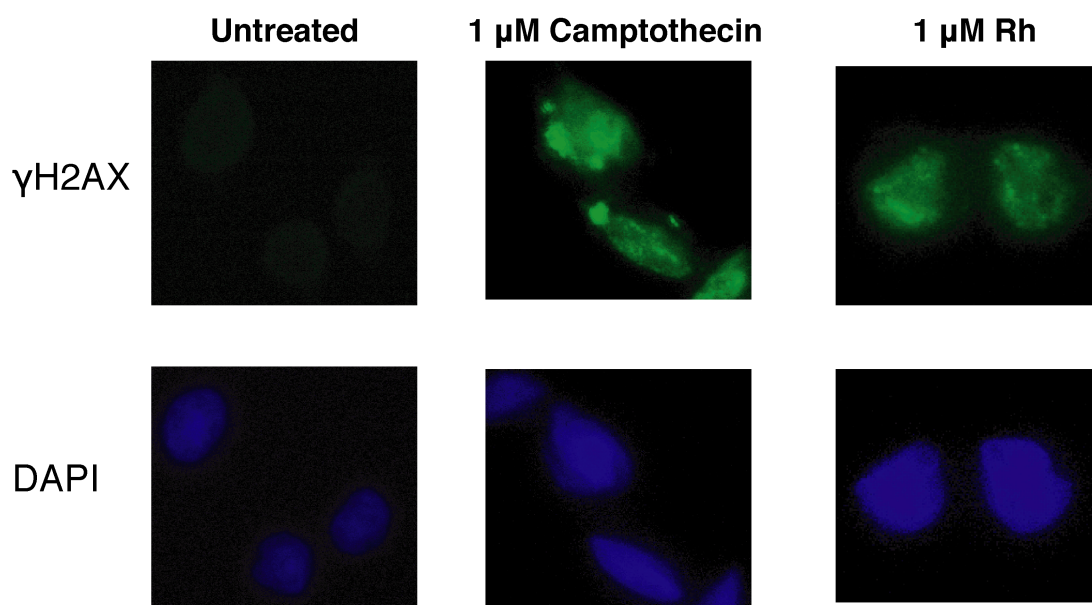


Figure 6.2 Confocal microscopy of immunofluorescence for γ H2AX (green) and nuclear staining with DAPI (blue) in fixed MMR-deficient HCT1160 cells after 2h exposure to 1 μ M camptothecin or $[\text{Rh}(\text{chrysi})(\text{phen})(\text{PPO})]^{2+}$.

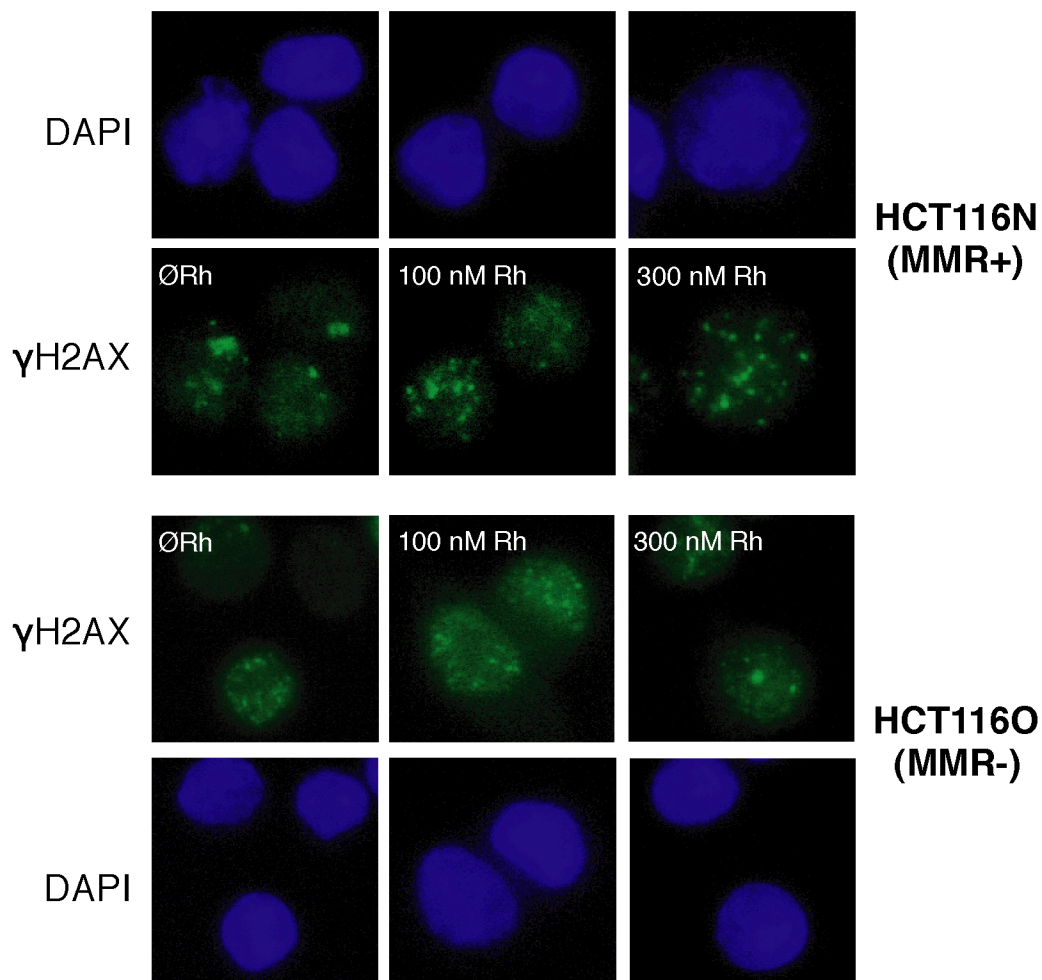


Figure 6.3 Confocal microscopy of immunofluorescence for γ H2AX (green) and nuclear staining with DAPI (blue) in fixed MMR-proficient HCT116N (top) and MMR-deficient HCT116O (bottom) cells after 2h exposure to 0, 100, or 300 nM $[\text{Rh}(\text{chrysi})(\text{phen})(\text{PPO})]^{2+}$.

nuclear pan-staining as well as γ H2AX foci in both cell types. It is possible that the incidence of γ H2AX foci in untreated cells is the result of inherent DNA damage arising from chromosomal instability or mutagenesis in these cancerous cells. Cells treated with 100 nM rhodium display similar fluorescence staining to that of untreated cells. The addition of 300 nM resulted in more observable γ H2AX foci, marginally above background pan-staining.

The appearance of γ H2AX foci occurs rapidly, after only two hours exposure to rhodium. This implies that metalloinsertor complexes trigger a cellular response almost immediately upon entry into the nucleus. It is surprising, however, that evidence of DNA damage arises in both MMR-proficient and MMR-deficient cells in response to rhodium treatment, when antiproliferative and cytotoxic effects are only observed in the MMR-deficient cell line. We considered the possibility that γ H2AX accumulates as an early response to the foreign rhodium complexes surrounding the genome, but postulated that the amount of γ H2AX may vary between the cell lines if allowed to recover in medium absent of rhodium. HCT116N and HCT116O cells were treated with 300 nM metalloinsertor for 2h and allowed to grow in fresh media for 6, 12, or 24h. Cells were then stained for γ H2AX and imaged by confocal immunofluorescence microscopy. **Figure 6.4** shows the induction of γ H2AX in HCT116N and HCT116O cells over time. Quantitation of foci in both cell lines was carried out, and cells were designated either as γ H2AX-negative (having zero foci), low- γ H2AX (1-5 foci per cell), moderate- γ H2AX (6-10 foci per cell), or high- γ H2AX (>10 foci per cell). As can be seen in **Figure 6.5**, the number of γ H2AX foci does vary in both cell lines over time, with either zero or low-foci counts in cells fixed immediately after treatment (“0 hr”), followed by an increase in the

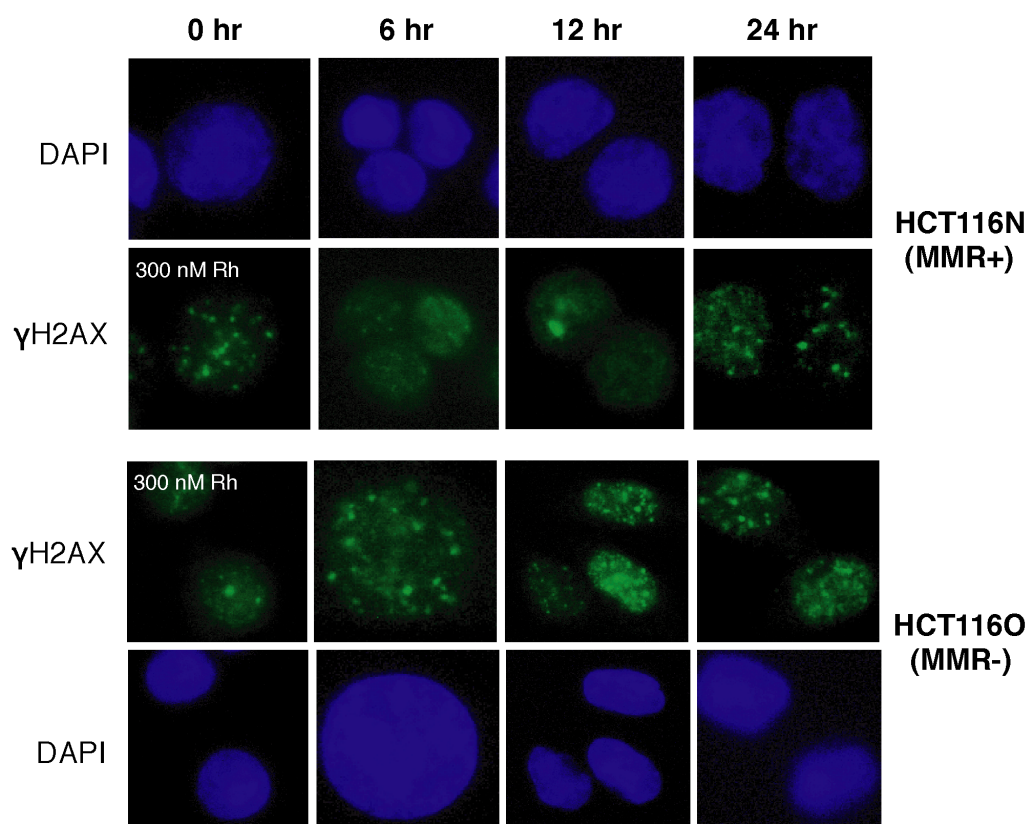


Figure 6.4 Confocal microscopy of immunofluorescence for γ H2AX (green) and nuclear staining with DAPI (blue) in fixed MMR-proficient HCT116N (top) and MMR-deficient HCT116O (bottom) cells after 2h exposure to 300 nM $[\text{Rh}(\text{chrysi})(\text{phen})(\text{PPO})]^{2+}$, followed by growth in non-rhodium containing medium for 6, 12, or 24h prior to fixation and staining. The “0 hr” time point refers to cells that were fixed immediately after rhodium treatment.

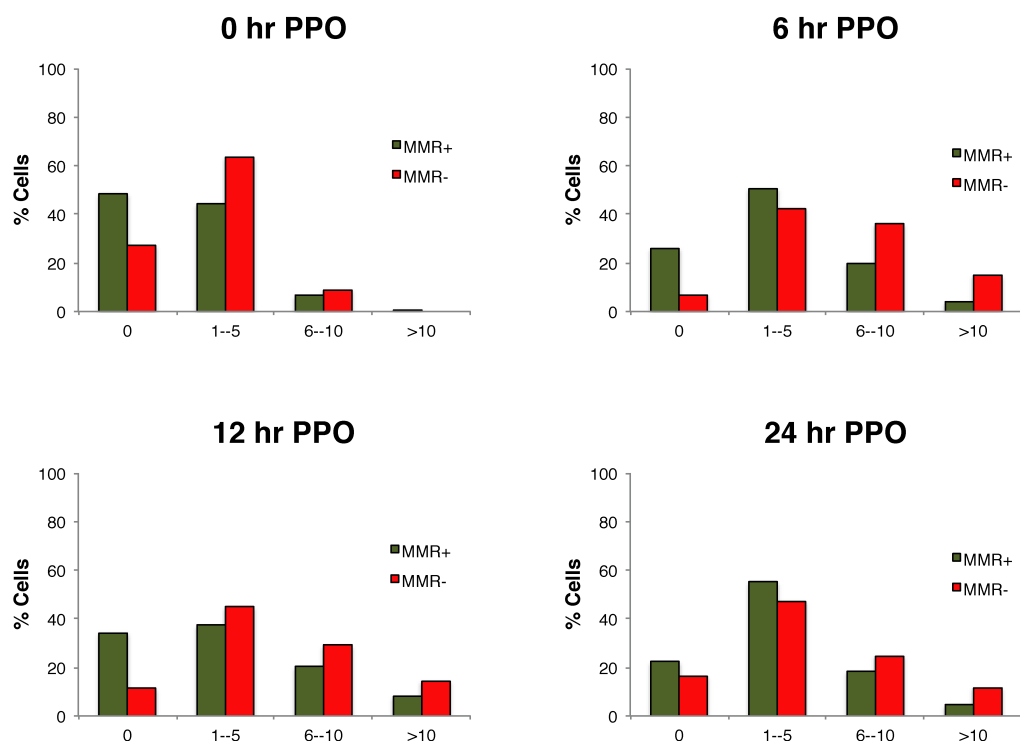


Figure 6.5 Quantitation of γ H2AX foci in HCT116N (MMR+, green) and HCT116O (MMR-, red) cells over time. Cells were exposed to $[\text{Rh}(\text{chrysi})(\text{phen})(\text{PPO})]^{2+}$ (300 nM) for 2h. After the treatment period, rhodium-containing medium was removed, replaced with fresh medium, and allowed to incubate for an additional 6, 12, or 24h. In the case of the 0 hr time point, cells were fixed immediately after rhodium treatment. Foci were quantified in each cell and designated as γ H2AX-negative (0 foci), low- γ H2AX (1-5 foci/cell), moderate- γ H2AX (6-10 foci/cell), or high- γ H2AX (>10 foci/cell). The percentage of each cell type was calculated as a fraction of the total cells in the images collected for each sample. For each sample, 3-5 images ($n = 30-150$ cells) were collected.

percentage of moderate- to high-foci counts after 6 and 12h recovery. The percentage of highly γ H2AX-positive cells decreases slightly in both cell lines between 12 and 24h.

To examine whether there was any difference in the γ H2AX response in HCT116N versus HCT116O cell lines, we calculated the percentage of combined moderate- and high- γ H2AX foci in each cell line (as a fraction of the total cells in each sample) over time – that is, cells containing ≥ 6 foci each were considered to be above background (γ H2AX-positive) based upon the quantification of γ H2AX in untreated cells (*vide infra*). As can be seen in **Figure 6.6**, there is a slight increase in the percentage of γ H2AX-positive cells in HCT116O cells (“MMR-”) versus HCT116N cells (“MMR+”) treated with rhodium, with 7 – 28% γ H2AX-positive HCT116N cells, and 9 – 52% γ H2AX-positive HCT116O cells. The trends in γ H2AX induction over time are also illustrated more clearly: an increase in double-strand breaks occurs 0 – 6h after rhodium exposure and remains steady from 6 – 12h. Between 12 and 24h, a slight decrease in γ H2AX is observed, possibly as a result of cell death.

Figure 6.6 also shows the time course data for camptothecin (“CT”) and untreated cells. Cells displaying moderate- to high- γ H2AX foci (≥ 6 foci/cell) were calculated as a percentage of total cells in the collection of images for each sample. As expected, a high percentage of cells treated with camptothecin are γ H2AX-positive across all time points. In HCT116N cells, the percentage of γ H2AX-positive cells remains constant between 0 – 12h, with a large increase ($>96\%$) at 24h. In contrast, the HCT116O cells treated with camptothecin follow a pattern similar to those treated with metalloinsertor: an increase from 0 – 6h (90 – 92%) followed by a decrease at 24h (66%). The full quantification of camptothecin-treated and untreated cells over time are depicted

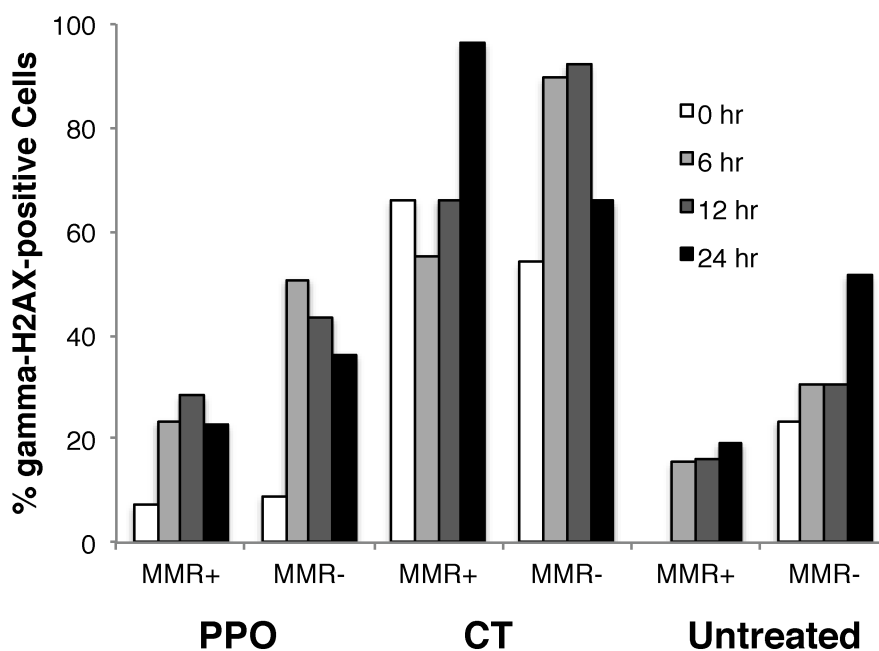


Figure 6.6 Quantitation of γ H2AX-positive cells in HCT116N (MMR+) and HCT116O (MMR-) cells treated with $[\text{Rh}(\text{chrysi})(\text{phen})(\text{PPO})]^{2+}$ (PPO, 300 nM) or camptothecin (CT, 1 μM) for 2h followed by growth in media absent of drug for a period of 6, 12, or 24h. For each time point, an untreated control was included, as well as a 0 hr time point in which treated cells were fixed immediately after drug exposure. Cells containing ≥ 6 foci/cell were designated as γ H2AX-positive, and the percentage of γ H2AX-positive cells was calculated as a fraction of the total cells in the images collected for each sample. For each sample, 3-5 images ($n = 30$ -150 cells) were collected.

in **Figure 6.7**. The untreated cells exhibit lower percentages of γ H2AX-positivity compared to treated cells, although γ H2AX staining is higher in the HCT116O cell line (24 – 52%) than in the HCT116N line (15 – 19%). This is possibly due to the incidence of DSBs arising spontaneously from microsatellite instability and a lack of mismatch repair. Additionally, DSBs may also occur as a result of chromosomal instability, as both cell types are transfected with an extra chromosome. Due to the relatively high occurrence of γ H2AX and DSBs in untreated cells, it is difficult to determine whether rhodium metalloinsertors in fact play a meaningful role in triggering γ H2AX induction in treated cells. Further studies are required to ascertain the statistical significance of these results.

6.3.1.2 Induction of 53BP1 in HCT116 Cells

To further elucidate the mechanisms that respond to metalloinsertor treatment, we stained for additional proteins that signal DNA damage. Staining for replication protein A (RPA), which binds to single stranded DNA and is involved in homologous recombination,³³ and Fanconi anemia group D2 protein (FANCD2), which colocalizes with the BRCA1 complex involved in DNA DSB repair,³⁴ produced no discernable foci in rhodium-treated cells (data not shown). Staining for 53BP1, which promotes non-homologous end-joining-mediated repair of DSBs,³⁵ was successfully visualized for cells treated with $[\text{Rh}(\text{chrysi})(\text{phen})(\text{PPO})]^{2+}$ and camptothecin. **Figure 6.8** depicts the induction of 53BP1 in HCT116N and HCT116O cells treated with rhodium or camptothecin (as well as untreated cells) for 2h followed by fixation and costaining with DAPI and γ H2AX. Foci corresponding to 53BP1 localization are observed for both

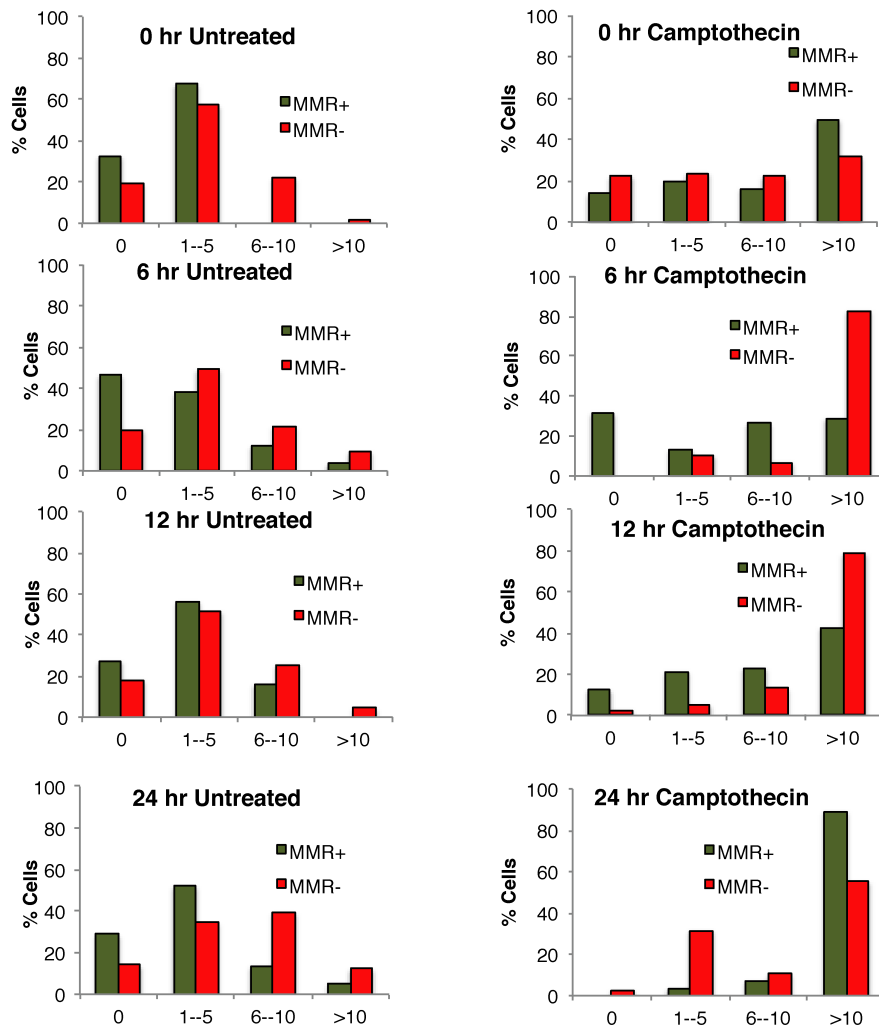


Figure 6.7 Quantitation of γ H2AX foci in HCT116N (MMR+, green) and HCT116O (MMR-, red) cells over time. Cells were untreated or exposed to camptothecin⁺ (1 μ M) for 2h, followed by growth in fresh media for an additional 6, 12, or 24h. In the case of the 0 hr time point, cells were fixed immediately after treatment. Foci were quantified in each cell and designated as γ H2AX-negative (0 foci), low- γ H2AX (1-5 foci/cell), moderate- γ H2AX (6-10 foci/cell), or high- γ H2AX (>10 foci/cell). The percentage of each cell type was calculated as a fraction of the total cells in the images collected for each sample. For each sample, 3-5 images ($n = 30$ -150 cells) were collected.

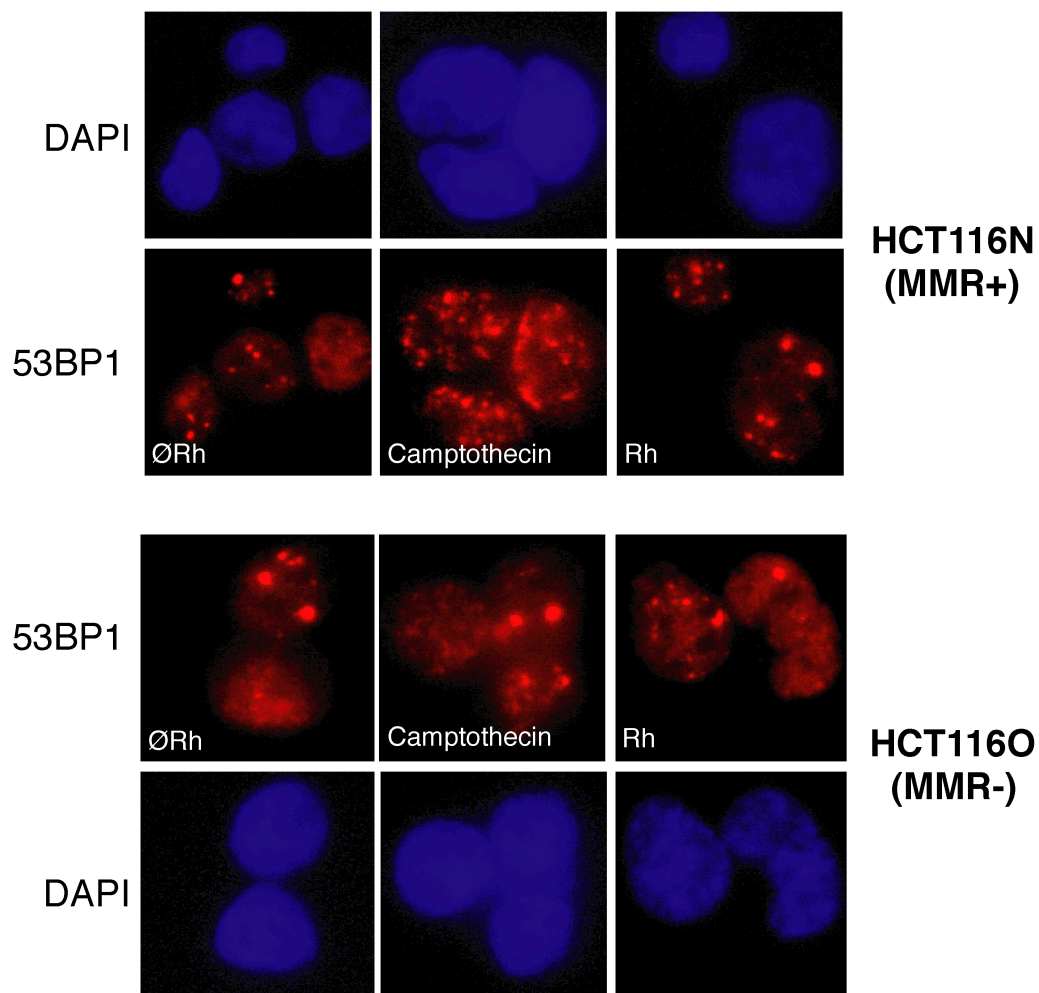


Figure 6.8 Confocal microscopy of immunofluorescence for 53BP1 (red) and nuclear staining with DAPI (blue) in fixed MMR-proficient HCT116N (top) and MMR-deficient HCT116O (bottom) cells after 2h exposure to camptothecin (1 μ M), [Rh(chrysi)(phen)(PPO)]²⁺ (“Rh,” 300 nM), or no treatment (ØRh).

MMR-proficient and MMR-deficient cells under all conditions, including untreated cells, again suggesting that the formation of DSBs may occur spontaneously in HCT116 cells.

Quantitative analysis of 53BP1 staining is shown in **Figure 6.9** and **Figure 6.10**. **Figure 6.9** displays the percentage of cells at each time point designated either as 53BP1-negative (having zero foci), low-53BP1 (1-5 foci per cell), moderate-53BP1 (6-10 foci per cell), or high-53BP1 (>10 foci per cell). Percentages were calculated as a fraction of the total number of cells in the collection of images for each sample. Accumulation of 53BP1 is less pronounced than γ H2AX for both rhodium- and camptothecin-treated cells. The majority of metalloinsertor-treated cells display low-53BP1, with 1 – 5 foci/cell, similar to that of untreated cells. The percentage of moderate- to high-53BP1 cells, i.e., cells containing ≥ 6 foci/cell, was also calculated as a function of time, shown in **Figure 6.10**. The percentage of 53BP1-positive cells treated with rhodium is equal to or lower than that of untreated cells at several time points, especially at 6 and 12h. Moreover, the difference in 53BP1 staining in Rh-treated HCT116N versus HCT116O cells is slight. These results suggest that metalloinsertor treatment has little effect on the induction of 53BP1 in HCT116 cells, signifying that this protein and the BRCA1 pathway are likely not associated with the cellular processing of mismatch recognition.

6.3.2 MTT Cytotoxicity Assay

The cytotoxic effects of $[\text{Rh}(\text{chrysi})(\text{phen})(\text{PPO})]^{2+}$ have been characterized previously in HCT116N and HCT116O cells, but the effects of camptothecin in these matched cell lines has not, to our knowledge, been explored. We performed an MTT cytotoxicity assay (MTT = (3-(4,5-dimethylthiazol-2-yl)-2,5-diphenyltetrazolium bromide) to ascertain the toxicity of camptothecin in the matched cell lines. Cells were

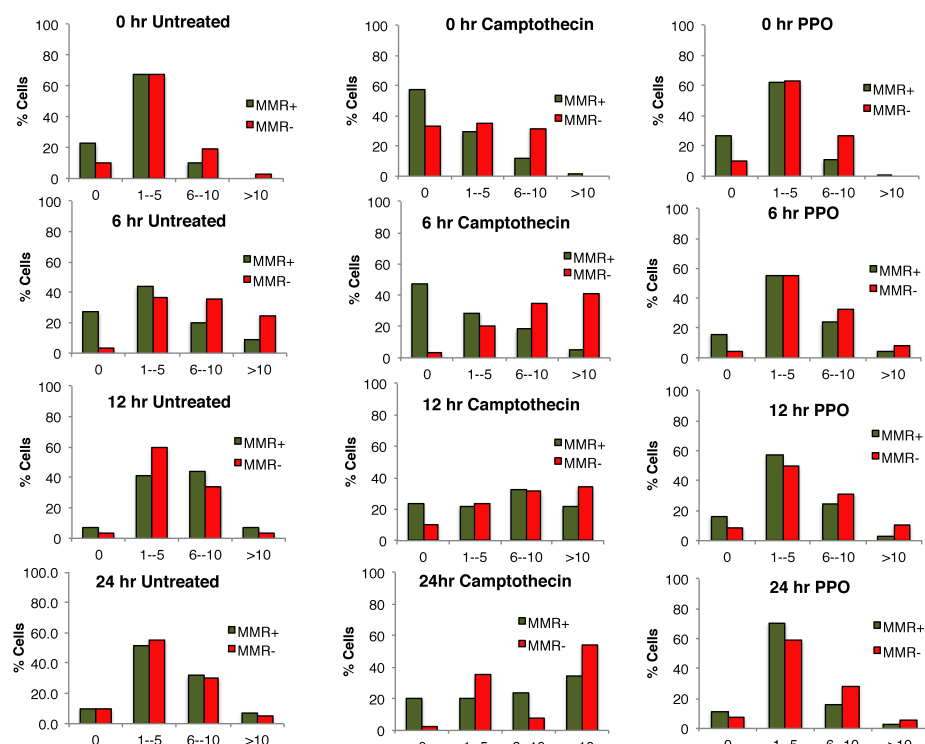


Figure 6.9 Quantitation of 53BP1 foci in HCT116N (MMR+, green) and HCT116O (MMR-, red) cells over time. Cells were either untreated or exposed to camptothecin (1 μ M) or [Rh(chrysi)(phen)(PPO)]²⁺ (300 nM) for 2h. After the treatment period, drug-containing medium was removed, replaced with fresh medium, and allowed to incubate for an additional 6, 12, or 24h. In the case of the 0 hr time point, cells were fixed immediately after treatment. Foci were quantified in each cell and designated as 53BP1-negative (0 foci), low-53BP1 (1-5 foci/cell), moderate-53BP1 (6-10 foci/cell), or high-53BP1 (>10 foci/cell). The percentage of each cell type was calculated as a fraction of the total cells in the images collected for each sample. For each sample, 3-5 images ($n = 30$ -150 cells) were collected.

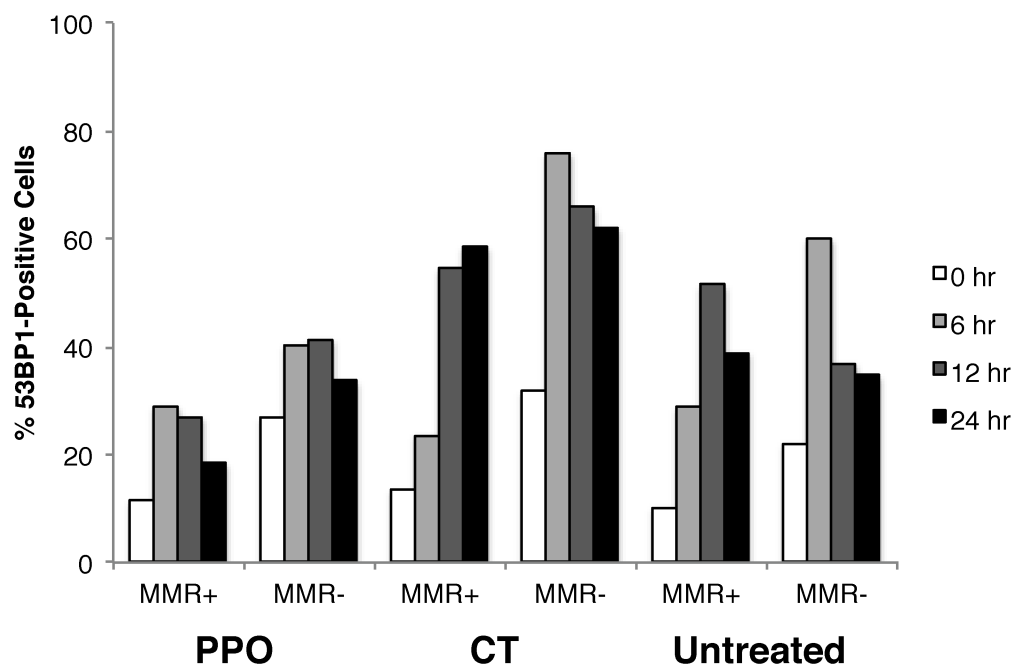


Figure 6.10 Quantitation of 53BP1-positive cells in HCT116N (MMR+) and HCT116O (MMR-) cells treated with $[\text{Rh}(\text{chrysi})(\text{phen})(\text{PPO})]^{2+}$ (PPO, 300 nM) or camptothecin (CT, 1 μM) for 2h followed by growth in media absent of drug for a period of 6, 12, or 24h. For each time point, an untreated control was included, as well as a 0 hr time point in which treated cells were fixed immediately after drug exposure. Cells containing ≥ 6 foci/cell were designated as 53BP1-positive, and the percentage of 53BP1-positive cells was calculated as a fraction of the total cells in the images collected for each sample. For each sample, 3-5 images ($n = 30-150$ cells) were collected.

plated in 96-well plates at 5.0×10^4 cells/well and treated with varying concentrations of $[\text{Rh}(\text{chrysi})(\text{phen})(\text{PPO})]^{2+}$ or camptothecin, for 72h under humidified atmosphere. Percent viability is defined as the ratio of the amount of formazan in treated cells to that of untreated cells. The cytotoxic effects of the complexes in the HCT116N and HCT116O cell lines are shown in **Figure 6.11**.

The metalloinsertor complex performs as expected, inducing cell-selective death in the HCT116O cell line with a peak differential cytotoxicity (defined as the difference in viability between the two cell lines) of $49 \pm 1.4\%$, occurring at 400 nM. The IC_{50} value (indicating the concentration at which 50% of the cells are viable) in HCT116O cells is approximately 200 nM, consistent with previous reports.²⁹ In contrast, camptothecin displays no preference for either cell line. Camptothecin exhibits moderate potency in both cell lines at the concentrations studied; after 72h at 1 μM exposure, $67 \pm 1.3\%$ of HCT116N cells remained viable, and $58 \pm 8.9\%$ of HCT116O cells were viable. While considerably less potent than $[\text{Rh}(\text{chrysi})(\text{phen})(\text{PPO})]^{2+}$ (which, at 1 μM after 72h, leaves $44 \pm 2.8\%$ and $13 \pm 0.5\%$ viability in HCT116N and HCT116O cells, respectively), camptothecin is clearly capable of inducing cytotoxic effects at the concentrations explored in the immunofluorescence assay. Additionally, the lack of preferential targeting by camptothecin is consistent with the occurrence of γH2AX -positive cells in both cell lines.

6.3.3 Metalloinsertors Induce Double Strand Breaks in the Genome of MMR-deficient Cells: Comet Assay

Immunofluorescence staining of MMR-proficient and MMR-deficient cells revealed that a DNA damage response is rapidly elicited upon exposure to low

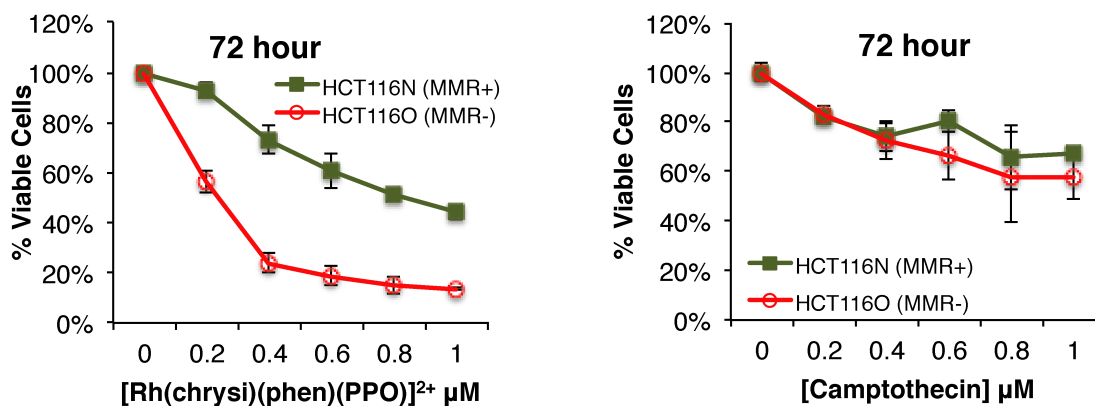


Figure 6.11 MTT cytotoxicity assay of HCT116N (MMR-proficient) and HCT116O (MMR-deficient) cells treated with $[\text{Rh}(\text{chrysi})(\text{phen})(\text{PPO})]^{2+}$ (left), and camptothecin (right). Cells were incubated with each complex at the concentrations indicated for 72h. After the incubation period, cells were treated with the MTT reagent for 4 h, and the resulting formazan crystals were solubilized with acidified SDS. Percent cell viability is defined as the percentage of formazan normalized to that of untreated cells. Standard errors were calculated from 5 replicates.

concentrations of rhodium. However, these assays do not indicate whether metalloinsertors directly damage the DNA themselves. We performed single-cell gel electrophoresis (“comet” assay) on HCT116N and HCT116O cells seeded in 6-well plates at 2×10^5 cells/well and treated with 500 nM $[\text{Rh}(\text{chrysi})(\text{phen})(\text{PPO})]^{2+}$ for 24h. Cells were harvested, washed with PBS, and embedded in low-melting agarose at 37 °C. The cell-agarose mixture was plated onto 3-well microscope slides, lysed with detergent, and electrophoresed under alkaline conditions (300 mM NaOH, 1 mM EDTA, pH >13). Cells were stained with fluorescent DNA-binding dye and analyzed by epifluorescence microscopy ($\lambda_{\text{ex}} = 488$ nm).

The results of the comet assay are depicted in **Figure 6.12**. Lysis conditions involving detergent and high salt concentrations condense undamaged DNA into supercoiled loops in the nucleus, which appear in the image as the heads of the “comet.” DNA containing DSBs becomes uncoiled under the alkaline electrophoresis conditions, thus migrating away from the supercoiled DNA in the gel matrix. Damaged DNA, thus, appears as the “comet tail” in the microscopy image. Remarkably, $[\text{Rh}(\text{chrysi})(\text{phen})(\text{PPO})]^{2+}$ induces DSBs in the DNA of HCT116O cells, but not the HCT116N cells. Comet tails indicating damaged DNA extend away from the supercoiled DNA head, having migrated towards the anodic end of the gel (to the right side of the image). These tails are also observed in cells treated with 500 nM camptothecin. The HCT116N cells containing rhodium largely resemble those of the untreated cells, with little evidence of damage in the form of tails. Untreated samples were run for both HCT116N and HCT116O cells; however, images were only collected for the HCT116O cell line due to photobleaching in the N-cell line.

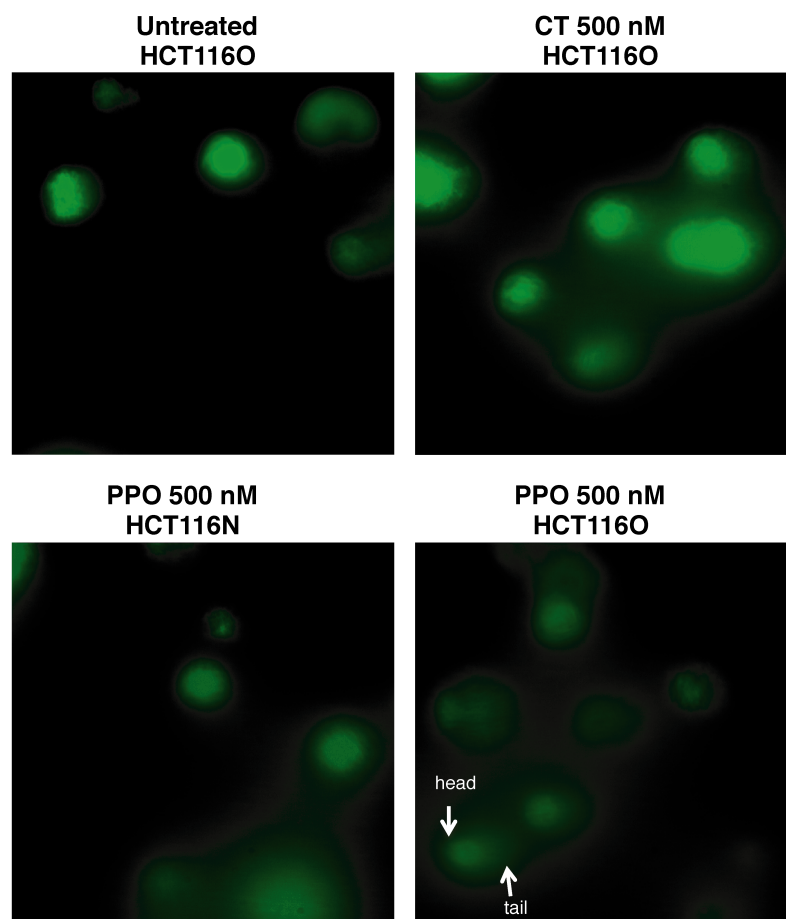


Figure 6.12 Single cell gel electrophoresis of HCT116N (left) and HCT116O (right) cells. Cells were plated at 2×10^5 and treated with 500 nM of either camptothecin or PPO for 24 h. Cells were harvested by trypsinization, washed, and mixed with OxiSelect agarose. Following lysis and alkaline treatment, slides were electrophoresed in alkaline buffer at 20 V (450 mA), stained with VistaGreen DNA dye, and imaged using epifluorescence microscopy, with excitation at 488 nm. Top: Untreated HCT116O cells (“CT,” left), HCT116O cells treated with 500 nM camptothecin. Bottom: HCT116N cells treated with $[\text{Rh}(\text{chrysi})(\text{phen})(\text{PPO})]^{2+}$ (“PPO,” left); HCT116O cells treated with PPO (right). Undamaged DNA is supercoiled to form the comet “head,” while damaged DNA migrates from left to right in the gel matrix, forming the comet “tail” (denoted by white arrows).

The results of the comet assay are consistent with what has been observed in assays of the antiproliferative and cytotoxic effects of metalloinsertors in these cell lines: these complexes would be expected to bind the DNA of the MMR-deficient HCT116O cells as they contain more mismatches than DNA in the corresponding HCT116N line. Yet it is surprising that these complexes are capable of inducing DNA strand breaks, as no evidence of damage has been observed in *in vitro* DNA binding experiments, particularly in the absence of UV light.²⁹ Furthermore, these results are inconsistent with those observed for the immunofluorescence assay, where the localization of DNA damage response proteins such as γ H2AX is observed for both cell lines. Clearly, there are additional response elements at play in the cellular processing of mismatch recognition by metalloinsertors.

6.3.4 Fluorescence Detection of Nascent RNA Synthesis *in Cellulo*

We next examined whether rhodium metalloinsertors inhibit transcription in MMR-deficient cells. HCT116N and HCT116O cells were seeded in 96-well plates at 4,000 cells/well and allowed 24h to adhere. Cells were then treated with either $[\text{Rh}(\text{chrysi})(\text{phen})(\text{PPO})]^{2+}$ (0 – 1 μM) or cisplatin (0 – 10 μM) for 24h. Cisplatin was chosen as a control because it is known to induce apoptosis in cells via inhibition of transcription. Cells were then pulse-chased for 1h with 1 mM ethynyl uridine (EU), which is incorporated into newly synthesized RNA indiscriminately in place of uridine. EU is not incorporated into DNA, so the amount of EU in the cells is reflective of the amount of RNA synthesis relative to untreated controls. After fixation, cells were labeled via copper-catalyzed click reaction with an azide-modified fluorophore. The amount of EU incorporation was quantified by fluorescence detection with excitation at 495 nm and

emission at 519 nm. The extent of transcription is expressed as the ratio of fluorescently labeled EU of cells treated with rhodium or platinum as compared to untreated controls.

As can be seen in **Figure 6.13**, $[\text{Rh}(\text{chrysi})(\text{phen})(\text{PPO})]^{2+}$ selectively inhibits transcription in the HCT116O cell line. The peak differential inhibition, defined as the difference in EU incorporation between the two cell lines, is $49 \pm 3.9\%$, occurring at 800 nM after 24 h. The rhodium complex has little effect on the amount of RNA synthesized in the HCT116N cell line. Cisplatin displays only modest inhibition of transcription ($90 \pm 16\%$ and $82 \pm 4.9\%$ at 10 μM in the HCT116N and HCT116O lines, respectively) and does not preferentially target either cell line. These results imply that the preferential inhibition of transcription by rhodium in MMR-deficient cells is the result of mismatch recognition in genomic DNA.

6.3.5 Rhodium Accumulation in Tumors

Preliminary *in vivo* studies in collaboration with Amgen have begun to explore the effect of metalloinsertor treatment on mice that have been implanted with MMR-deficient HCT116 tumor xenografts. Tumors were harvested from the mice after 24h dosage and nuclear and cytosolic lysates were extracted via differential centrifugation procedures. The soluble fractions were analyzed for rhodium content by inductively coupled plasma mass spectrometry (ICP-MS) and normalized to protein content as determined by bicinchoninic acid (BCA) assay. Rhodium concentration is thus expressed as ng [Rh]/mg [soluble protein]. The insoluble tumor fractions, including membranes and connective tissue, could not be sufficiently solubilized for ICP-MS and thus were not analyzed for rhodium content.

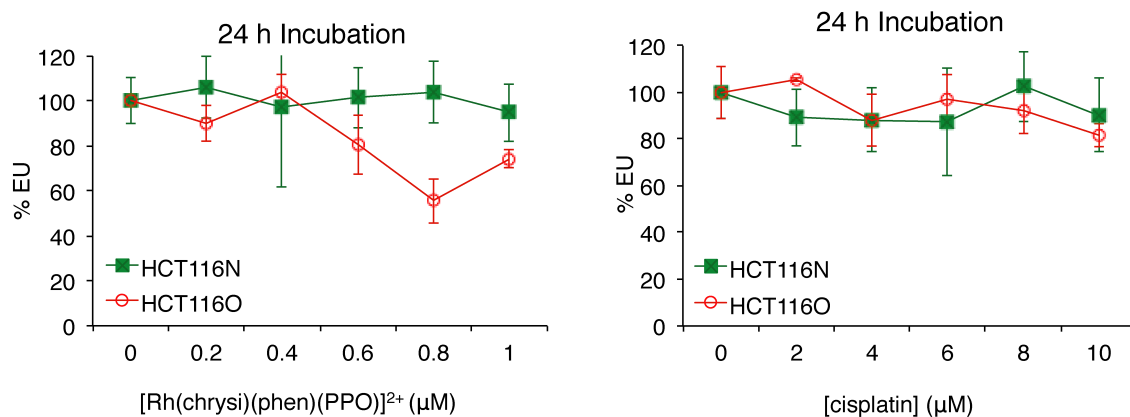


Figure 6.13 Analysis of RNA synthesis in HCT116N (green) and HCT116O (red) cells as a function of $[\text{Rh}(\text{chrysi})(\text{phen})(\text{PPO})]^{2+}$ or cisplatin concentration after 24h. Cells were plated at 4,000 cells/well in 96-well plates. RNA synthesis is expressed as the percentage EU incorporation normalized to the untreated samples. Percent errors are calculated from 5 replicates.

The results are summarized in **Figure 6.14**. Tumor samples for mice treated with 100 mg/kg $[\text{Rh}(\text{HDPa})_2\text{chrysi}]^{3+}$ and $[\text{Rh}(\text{chrysi})(\text{phen})(\text{PPE})]^{2+}$ could not be obtained due to the extreme toxicity of the dosage. Only the controls (PBS only and Cdc7 inhibitor) and the low-dose samples of $[\text{Rh}(\text{chrysi})(\text{phen})(\text{PPE})]^{2+}$ and $[\text{Rh}(\text{chrysi})(\text{phen})(\text{PPO})]^{2+}$ yielded soluble tumor lysate that was suitable for analysis by ICP-MS. High variability was observed within each group of mice. Background rhodium was determined by running samples of 1% $\text{HNO}_{3(\text{aq})}$ through the instrument, which yielded a baseline concentration of 0.11 ± 0.01 ppb Rh. Because the overall rhodium concentrations are low for tumor samples, concentrations are also provided in ppb (**Table 6.2**) to determine whether normalized samples are sufficiently above background.

Unsurprisingly, tumors dosed with only PBS displayed no appreciable rhodium content with < 0.05 ng [Rh]/mg [soluble protein] – well below background. Similarly, mice treated with only Cdc7 inhibitor displayed no rhodium content; one of the replicates appears to display high rhodium content when normalized to protein concentration, but Rh concentration in ppb is below baseline. Two of the three mice treated with 10 mg/kg $[\text{Rh}(\text{chrysi})(\text{phen})(\text{PPE})]^{2+}$ displayed rhodium accumulation well above background, with approximately 0.38 and 0.25 ng [Rh]/mg [soluble protein], while the third mouse in the group displayed rhodium slightly above baseline (0.14 ng [Rh]/mg [soluble protein]). Additionally, all but one of the mice treated with $[\text{Rh}(\text{chrysi})(\text{phen})(\text{PPO})]^{2+}$ showed signs of rhodium uptake into the tumor grafts: dosage at 10 mg/kg $[\text{Rh}(\text{chrysi})(\text{phen})(\text{PPO})]^{2+}$ yielded 0.04 ng [Rh]/mg [soluble protein] (below baseline) and 0.23 ng [Rh]/mg [soluble protein] (above baseline); soluble tumor lysate from the third mouse in this group could not be procured. For the 20 mg/kg dosage of

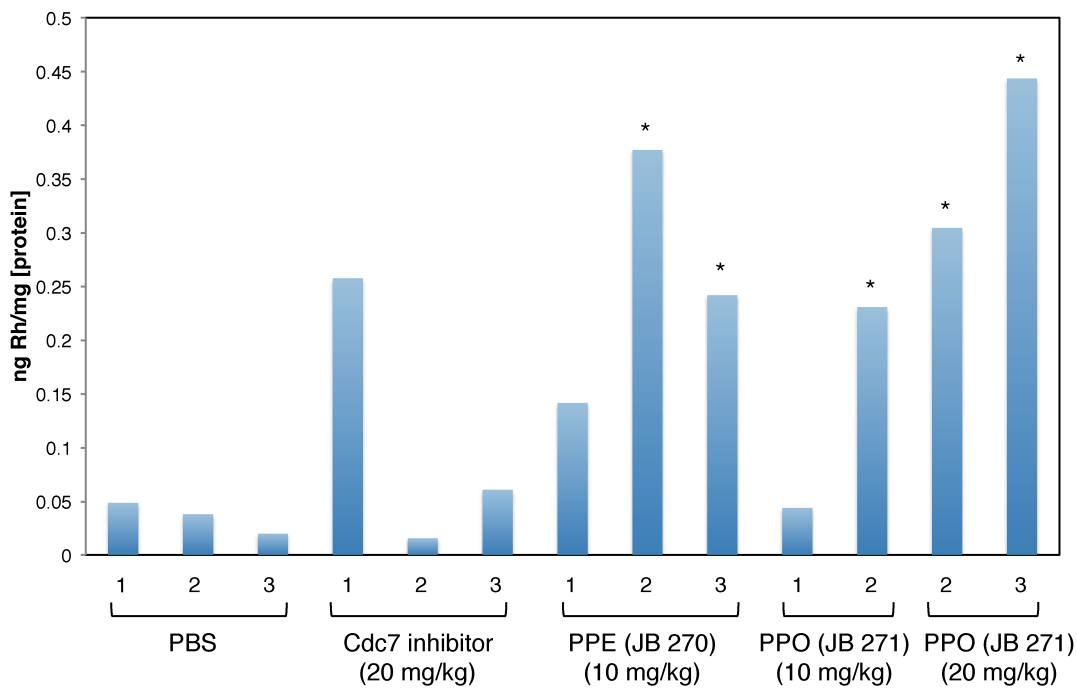


Figure 6.14 Rhodium accumulation in human HCT116 tumors harvested from nude mice. Groups of mice were dosed in triplicate with the indicated compounds for 24h. Tumor samples were lysed, separated from the insoluble content, and the soluble fractions were analyzed for rhodium uptake by ICP-MS. Rhodium content was normalized to protein concentration as determined by BCA analysis, and is expressed as ng Rh/ mg [soluble protein]. Samples containing rhodium determined to be above background are denoted by the asterisks.

[Rh(chrysi)(phen)(PPO)]²⁺ tumor samples were only harvested for two of the three mice in the group. Lysates from both samples, however, displayed some of the highest rhodium accumulation, with 0.30 and 0.44 ng [Rh]/mg [soluble protein]. Additionally, there is evidence for dose-dependent accumulation of [Rh(chrysi)(phen)(PPO)]²⁺ in these tumors.

Overall, HCT116 tumor xenografts implanted in live mice exhibit modest rhodium accumulation, but it is clear that at least some of the metalloinsertor is reaching the tumor in a complex, multicellular environment. However, the accumulation of rhodium in tumors *in vivo* is not sufficient to reach the concentrations required for cellular activity. The development of metalloinsertor conjugates with cell- and tissue-targeting functionalities may assist in improving the biodistribution of metalloinsertors *in vivo*.

Table 6.2 Rhodium Accumulation in HCT116 Tumors^a

Sample ^b	[Rh] ppb	Comparison to Baseline ^a
PBS – 1	0.04	—
PBS – 2	0.02	—
PBS – 3	0.03	—
Cdc7 inhibitor – 1	0.08	—
Cdc7 inhibitor – 2	0.01	—
Cdc7 inhibitor – 3	0.06	—
[Rh(chrysi)(phen)(PPE)] ²⁺ – 1	0.08	—
Rh(chrysi)(phen)(PPE)] ²⁺ – 2	0.30	+
Rh(chrysi)(phen)(PPE)] ²⁺ – 3	0.27	+
Rh(chrysi)(phen)(PPO)] ²⁺ (10 mg/kg) – 1	0.03	—
Rh(chrysi)(phen)(PPO)] ²⁺ (10 mg/kg) – 2	0.24	+
Rh(chrysi)(phen)(PPO)] ²⁺ (20 mg/kg) – 2	0.18	+
Rh(chrysi)(phen)(PPO)] ²⁺ (20 mg/kg) – 3	0.62	+

^aRhodium accumulation in HCT116 tumors expressed in ppb is compared to background rhodium concentration in blank samples (1% HNO_{3(aq)}), determined to be 0.11 ± 0.01 ppb. A “—” indicates that the rhodium concentration measured for each sample lies below the baseline rhodium in blank 1% HNO_{3(aq)} samples. ^bEach dosage was carried out on groups of three mice, denoted by the numbers next to each sample.

6.4 Discussion

6.4.1 Metalloinsertors Damage Genomic DNA

Biological characterization of metalloinsertors in the isogenically matched HCT116N and HCT116O cells has established that these complexes inhibit DNA synthesis, induce cell cycle arrest, and trigger necrosis selectively in cells exhibiting MMR-deficiency – that is, cells with DNA containing approximately 1000 fold more base pair mismatches than the DNA of MMR-proficient cells. Examination of metalloinsertor subcellular localization subsequently revealed that this cell-selectivity is dependent upon uptake into the nucleus, rather than the mitochondria, further supporting the hypothesis that the biological activity of these complexes is derived from mismatch recognition in genomic DNA. However, direct evidence of interaction between metalloinsertors and the genome has not previously been obtained. Immunofluorescence staining of MMR-proficient and MMR-deficient cells revealed that metalloinsertors induce a rapid DNA damage response (2 hours) at low concentrations (300 nM), in the form of focal accumulation of γ H2AX.

The H2AX protein is a component of the H2A histone family and contributes to nucleosome formation. When the genome undergoes DNA damage, particularly in the form of DSBs, H2AX becomes phosphorylated on serine 139 to form γ H2AX, which in turn localizes and recruits DNA repair proteins to points of injury. As such, γ H2AX focal accumulation is an important biomarker for chromosomal damage and could reveal information about the downstream processes associated with rhodium treatment. Immunofluorescence staining of HCT116N and HCT116O cells has revealed that these cells, particularly the HCT116O line, appear to spontaneously induce γ H2AX foci even

in the absence of drug. This could potentially be a result of chromosomal instability arising from the transfection of chromosome 3 (in HCT116N cells) and chromosome 2 (in HCT116O cells); aneuploid cells are highly susceptible to chromosomal aberrations.³⁶ Additionally, the occurrence of DSBs in untreated HCT116O cells may be a result of the lack of MMR, as microsatellite instability can lead to DNA damage and mutations in DNA repair proteins.³⁷

Despite the presence of γ H2AX foci in untreated cells, the addition of $[\text{Rh}(\text{chrysi})(\text{phen})(\text{PPO})]^{2+}$ produces substantially higher γ H2AX staining at sufficient concentrations. At 1 μM rhodium, fluorescence is similar to that of 1 μM camptothecin, indicating that metalloinsertors induce double strand breaks in the genome, possibly via direct interaction with the DNA through mismatch binding (**Figure 6.2**). However, γ H2AX foci also appear in HCT116N cells treated with rhodium, even though the PPO complex is not cytotoxic in the N-cell line.

To explore whether rhodium concentration played a role in incurring nonspecific DNA strand breaks, we carried out the staining with 100 nM and 300 nM $[\text{Rh}(\text{chrysi})(\text{phen})(\text{PPO})]^{2+}$. These concentrations were chosen because 100 nM is the lowest dose at which biological activity occurs, and 300 nM is roughly the concentration at which peak differential cytotoxicity (the difference in viability between the two cell lines) is observed.²⁹ The addition of 100 nM rhodium has little effect on cells, but 300 nM rhodium results in a small but measurable increase in γ H2AX foci compared to untreated cells.

We also examined the possibility that γ H2AX foci may simply occur as an early cellular response to the presence of rhodium, perhaps as it electrostatically associates

with the DNA, searching for a mismatch. If this were the case, foci could potentially appear in both cell lines immediately upon short-term exposure to rhodium, but may clear if cells did not acquire more permanent DNA damage. Cells were consequently treated with complex for 2h, but then allowed a “recovery” period in fresh media without rhodium. It was hypothesized that if γ H2AX was localizing to irreparable damage caused by the metalloinsertor, foci would still be present after the recovery period, but if γ H2AX foci were simply an early “alarm” signal, foci would clear once cells were allowed to grow again in the absence of complex. Indeed, γ H2AX foci do increase over time, and slightly more so in the MMR-deficient cell line than in the MMR-proficient line. For both cell lines, the most dramatic increase in the percentage of γ H2AX-positive cells occurs in the first 6h post-treatment. In the HCT116O cells, the percentage of γ H2AX-positive cells declines over the remainder of the 24h recovery period. One possible explanation is that the metalloinsertor is causing DNA damage that recruits a cellular response in the first 6h, but foci dissipate as the lesions are repaired. It is also possible that the decrease in foci over time is the result of cell cycle arrest and/or cell death – previous work has shown that metalloinsertors inhibit DNA synthesis as early as 6h, and cytotoxicity can be observed at 24h.

In general, the results of the immunofluorescence study exhibited only modest evidence of DNA damage compared to untreated cells as well as a slight preference for the MMR-deficient cell line. Further studies must be carried out to assess whether these current observations hold any significance. Additionally, we examined the effects of metalloinsertor treatment on DNA more directly using single cell gel electrophoresis, which electrophoretically separates damaged DNA from undamaged within a cell. We

observed that $[\text{Rh}(\text{chrysi})(\text{phen})(\text{PPO})]^{2+}$ treatment results in DSBs in HCT116O cells, but not HCT116N cells.

Mismatch repair deficiency appears to correlate with DNA double strand breaks upon treatment with rhodium metalloinsertors, but it is still unclear how metalloinsertion leads to these breaks. *In vitro* DNA binding studies of $[\text{Rh}(\text{chrysi})(\text{phen})(\text{PPO})]^{2+}$ have shown that the complex binds non-covalently and, like most metalloinsertors, do not induce sugar-phosphate backbone cleavage even with irradiation. Even photocleaving metalloinsertors, such as $[\text{Rh}(\text{bpy})_2\text{chrysi}]^{3+}$ and $[\text{Rh}(\text{bpy})_2\text{phzi}]^{3+}$, only lead to scission on one strand, and only at the mismatched sites.

Camptothecin also binds DNA non-covalently and induces DSBs that lead to γH2AX foci and cytotoxicity. This quinolone alkaloid forms highly specific hydrogen bonding contacts between DNA (at cytosine residues) and the DNA binding protein topoisomerase I (topo I). The resulting ternary complex of drug, DNA, and DNA cleavage enzyme results in stalled progression of topo I, leading to accumulation of DSBs in the genome as well as transcription inhibition.³² It is possible that metalloinsertors bound to DNA mismatches are also bound by proteins that recognize and attempt to repair the lesion, leading to an accumulation of DNA strand breaks and inhibition of transcription.

6.4.2 Metalloinsertors Inhibit Transcription in MMR-Deficient Cells

Perhaps more significantly than damaging the genome, metalloinsertors also inhibit RNA synthesis selectively in the HCT116O cell line. Inhibition of transcription is a key step in the anticancer activity of cisplatin: loss of the ability to synthesize messenger RNA prevents cells from entering mitosis, thus leading to cell cycle arrest in

the G2 phase.^{38,39} Early studies of metalloinsertor cytotoxicity revealed that HCT116O cells also undergo cell cycle arrest in the G2/M phase,²³ which could potentially arise from an inability to synthesize the mRNA necessary to pass into mitosis (M phase).

Cisplatin arrests transcription through the formation of covalent DNA adducts, which reduce the binding affinity of RNA polymerases and block elongation.^{40,41} It is remarkable, then, that metalloinsertors also possess such capabilities, given that their interaction with DNA is non-covalent. Previous examples of non-covalent DNA binding compounds have been shown to inhibit transcription. Synthetic polyamides that bind the minor groove of DNA with high sequence specificity block transcription by binding to the transcription factor TFIIIA binding site.⁴² Additionally, a sequence-selective rhodium intercalator complex bearing 4-guanidylmethyl-1,10-phenanthroline ligands blocks transcription factor binding from the major groove.⁴³ In these cases, however, the compounds bound DNA sequences spanning six or more base pairs – comparatively much larger areas than a single base mismatch. In the case of the metallointercalator complex, the DNA helix was also unwound 70°, in addition to steric inhibition of protein binding.⁴³ Metalloinsertors, in contrast, induce no such distortions to the overall structure of the duplex,^{16,19} although extrusion of mismatched bases from the base stack may preclude binding of proteins critical to transcription. Future studies will attempt to further elucidate the specific effects of metalloinsertors and mismatch binding on transcription.

6.4.3 Effects of Rhodium Metalloinsertors *in Vivo*

The development of more potent and more selective metalloinsertor complexes, such as $[\text{Rh}(\text{chrysi})(\text{phen})(\text{PPO})]^{2+}$ and $[\text{Rh}(\text{chrysi})(\text{phen})(\text{PPE})]^{2+}$, have led to efforts to explore the potential efficacy of these compounds *in vivo*. In collaboration with Amgen,

we have discovered that our complexes are stable in plasma and possess pharmacokinetic properties suitable for *in vivo* studies. Here, we examined the effects of metalloinsertor treatment on MMR-deficient tumors implanted in mice, and found tolerable dosages for our most active complexes. While further analysis has revealed that rhodium exposure levels were below the concentrations required for cellular activity, we have also shown that some of the metalloinsertor is in fact reaching the tumor, albeit in concentrations too low to have an effect. With the continued development of bifunctional conjugates, we aim to exert increased control over the biodistribution of these compounds. The appendage of cell- and tissue-specific elements, such as peptides and antibodies, are anticipated to enhance targeting of metalloinsertors in complex biological systems.

6.5 Conclusions

The synthesis of new generations of rhodium metalloinsertors has afforded complexes that target mismatch repair-deficient cells with increasing selectivity and unprecedented potency. With the discovery of metalloinsertors that exhibit cellular EC_{50} activities in the nanomolar range, the development of this class of complexes into clinically viable therapeutics becomes increasingly feasible. Efforts to uncover how the cell responds to mismatch recognition by our complexes in the nucleus have revealed that metalloinsertors selectively inhibit transcription in MMR-deficient cells, and likely cause double strand breaks to the genome. Furthermore, the cellular response to metalloinsertor treatment is rapid, with protein signaling occurring after only 2h. Preliminary *in vivo* mouse studies of rhodium metalloinsertors revealed that these complexes are tolerated at low doses and that the complex can accumulate in MMR-deficient tumors while traversing the complex environment of a multicellular organism. These biological studies,

though preliminary, show great promise for metalloinsertors as targeted chemotherapeutics for mismatch-repair deficient cancers.

6.6 References

- 1 Hoeijmakers, J. H. J. *Nature*. **2001**, *411*, 366-374.
- 2 Watson, J. D.; Baker, T. A.; Bell, S. P.; Gann, A.; Levine, M.; Losick, R. in *Molecular Biology of the Gene*, 5th ed. (Ed: Peason Benjamin Cummings), CSHL Press. **2004**, ch 9-10.
- 3 Wildenberg, J.; Meselson, M. *Proc. Nat. Acad. Sci. USA*. **1975**, *72*, 2202-2206.
- 4 Wagner, Jr., R.; Meselson, M. *Proc. Nat. Acad. Sci. USA*. **1976**, *73*, 4135-4139.
- 5 Iyer, R. R.; Pluciennik, A.; Burdett, V.; Modrich, P. L. *Chem. Rev.* **2006**, *106*, 302-323.
- 6 Parsons, R.; Li, G.-M.; Longley, M.; Modrich, P.; Liu, B.; Berk, T.; Hamilton, S. R.; Kinzler, K. W.; Vogelstein, B. *Science*. **1995**, *268*, 738-740.
- 7 Jiricny, J. *Nat. Rev. Mol. Cell Biol.* **2006**, *7*, 335-346.
- 8 Tzung, T. Y.; Diem, C.; Runger, T. M. *Arch. Dermatol. Res.* **1998**, *290*, 109-112.
- 9 N. Papadopoulos, A. Lindblom, *Hum. Mutat.* **1997**, *10*, 89–99.
- 10 I. I. Arzimanoglou, F. Gilbert, H. R. K. Barber, *Cancer*. **1998**, *82*, 1808–1820.
- 11 D. Fink, S. Aebi, S. B. Howell, *Clin. Cancer Res.* **1998**, *4*, 1-6.
- 12 R. J. Fram, P. S. Cusick, J. M. Wilson, M. G. Marinus, *Mol. Pharmacol.* **1985**, *28*, 51-55.
- 13 Weidmann, A. G.; Komor, A. C.; Barton, J. K. *Comments on Inorganic Chemistry* **2014**, *34*, 114-123.
- 14 Jackson, B. A.; Barton, J. K. *J. Am. Chem. Soc.* **1997**, *119*, 12986–12987.
- 15 Cordier, C.; Pierre, V. C.; Barton, J. K. *J. Am. Chem. Soc.* **2007**, *129*, 12287–12295.

- 16 Zeglis, B. M.; Pierre, V. C.; Kaiser, J. T.; Barton, J. K. *Biochemistry* **2009**, *48*, 4247–4253.
- 17 Jackson, B. A.; Alekseyev, V. Y.; Barton, J. K. *Biochemistry* **1999**, *38*, 4655–4662.
- 18 Jackson, B. A.; Barton, J. K. *Biochemistry* **2000**, *39*, 6176–6182.
- 19 Pierre, V. C.; Kaiser, J. T.; Barton, J. K. *Proc. Natl. Acad. Sci. U.S.A.* **2007**, *104*, 429–434.
- 20 Koi, M.; Umar, A.; Chauhan, D. P.; Cherian, S. P.; Carethers, J. M.; Kunkel, T. A.; Boland, C. R. *Cancer Res.* **1994**, *54*, 4308-4312.
- 21 Hart, J. R.; Glebov, O.; Ernst, R. J.; Kirsch, I. R.; Barton, J. K. *Proc. Natl. Acad. Sci. U.S.A.* **2006**, *103*, 15359–15363.
- 22 Ernst, R. J.; Song, H.; Barton, J. K. *J. Am. Chem. Soc.* **2009**, *131*, 2359–2366.
- 23 Ernst, R. J.; Komor, A. C.; Barton, J. K. *Biochemistry* **2011**, *50*, 10919–10928.
- 24 Komor, A. C.; Schneider, C. J.; Weidmann, A. G.; Barton, J. K. *J. Am. Chem. Soc.* **2012**, *134*, 19223–19233.
- 25 Weidmann, A. G.; Komor, A. C.; Barton, J. K. *Philos. Trans. R. Soc. A.* **2013**, *371*, 20120117.
- 26 Bailis, J. M.; Gordon, M. L.; Gurgel, J. L.; Komor, A. C.; Barton, J. K.; Kirsch, I. R. *PLoS One* **2013**, *8*, e78726.
- 27 Kuo, L. J.; Yang, L. X. *In Vivo* **2008**, *22*, 305-309.
- 28 Murner, H.; Jackson, B. A.; Barton, J. K. *Inorg. Chem.* **1998**, *37*, 3007–3012.

- 29 Komor, A. C.; Barton, J. K. *J. Am. Chem. Soc.* **2014**, *136*, 14160-14172.
- 30 Mosmann, T. *J. Immunol. Methods* **1983**, *65*, 55-63.
- 31 Smith, P. K.; Krohn, R. I.; Hermanson, G. T.; Mallia, A. K.; Gartner, F. H.; Provenzano, M. D.; Fujimoto, E. K.; Goeke, N. M.; Olson, B. J.; Klenk, D. C. *Anal. Biochem.* **1985**, *150*, 76-85.
- 32 Pommier, Y.; Redon, C.; Rao, V.A.; Seiler, J.A.; Sordet, O.; Takemura, H.; Antony, S.; Meng, L.; Liao, Z.; Kohlhagen, G. *Mutat. Res.* **2003**, *532*, 173-203.
- 33 Xuan, L.; Wolf-Dietrich, H. *Cell Res.* **2008**, *18*, 99-113.
- 34 Garcia-Higuera I.; Taniguchi, T.; Ganesan, S.; Meyn, M.S.; Timmers, C.; Hejna, J.; Grompe, M.; D'Andrea, A.D. *Mol. Cell.* **2001**, *7*, 249-262.
- 35 Panier, S.; Boulton, S. J. *Nat. Rev. Mol. Cell Biol.* **2014**, *15*, 7-18.
- 36 McCarthy, N. *Nat. Rev. Cancer* **2011**, *11*, 760.
- 37 Li, H. R.; Shagisultanova, E. I.; Yamashita, K.; Piao, Z.; Perucho, M.; Malkhosyan, S. R. *Cancer Res.* **2004**, *64*, 4760-4767.
- 38 Todd, R. C.; Lippard, S. J. *Metallomics* **2009**, *1*, 290-291.
- 39 Sandman, K. E.; Marla, S. S.; Zlokarnik, G.; Lippard, S. J. *Chem. Biol.* **1999**, *6*, 541-551.
- 40 Tornaletti, S.; Patrick, S. M.; Turchi, J. J.; Hanawalt, P.C. *J. Biol. Chem.* **2003**, *278*, 35791-35797.
- 41 Damsma, G. E.; Alt, A.; Brueckner, F.; Carell, T.; Cramer, P. *Nat. Struct. Mol. Biol.* **2007**, *14*, 1127-1133.
- 42 Gottesfeld, J. M.; Neely, L.; Trauger, J. W.; Baird, E. E.; Dervan, P. B. *Nature* **1997**, *387*, 202-205.

- 43 Odom, D. T.; Parker, C. S.; Barton, J. K. *Biochemistry*, **1999**, *38*, 5155-5163.